Demonstration of a State-Insensitive, Compensated Nanofiber Trap

A. Goban,[1] K. S. Choi,[1,2] D. J. Alton,[1] D. Ding,[1] C. Lacroûte,[1] M. Pototschnig,[1] T. Thiele,[1,*] N. P. Stern,[1,†] and H. J. Kimble[1]

[1]*Norman Bridge Laboratory of Physics 12-33, California Institute of Technology, Pasadena, California 91125, USA*
[2]*Spin Convergence Research Center 39-1, Korea Institute of Science and Technology, Seoul 136-791, Korea*

(Received 4 March 2012; published 19 July 2012)

We report the experimental realization of an optical trap that localizes single Cs atoms $\simeq 215$ nm from the surface of a dielectric nanofiber. By operating at magic wavelengths for pairs of counterpropagating red- and blue-detuned trapping beams, differential scalar light shifts are eliminated, and vector shifts are suppressed by ≈ 250. We thereby measure an absorption linewidth $\Gamma/2\pi = 5.7 \pm 0.1$ MHz for the Cs $6S_{1/2}$, $F = 4 \rightarrow 6P_{3/2}$, $F' = 5$ transition, where $\Gamma_0/2\pi = 5.2$ MHz in free space. An optical depth $d \simeq 66$ is observed, corresponding to an optical depth per atom $d_1 \simeq 0.08$. These advances provide an important capability for the implementation of functional quantum optical networks and precision atomic spectroscopy near dielectric surfaces.

DOI: 10.1103/PhysRevLett.109.033603 PACS numbers: 42.50.Ct, 37.10.Gh, 37.10.Jk, 42.50.Ex

An exciting frontier in quantum information science is the integration of otherwise "simple" quantum elements into complex quantum networks [1]. The laboratory realization of even small quantum networks enables the exploration of physical systems that have not heretofore existed in the natural world. Within this context, there is active research to achieve lithographic quantum optical circuits, for which atoms are trapped near micro- and nanoscopic dielectric structures and "wired" together by photons propagating through the circuit elements. Single atoms and atomic ensembles endow quantum functionality for otherwise linear optical circuits and, thereby, the capability to build quantum networks component by component.

Creating optical traps compatible with the modal geometries of micro- and nanoscopic optical resonators and waveguides [2,3] is a long-standing challenge in atomic, molecular, and optical physics [4–6]. "Optical tweezers" with tight focusing have succeeded in trapping single atoms within small volumes $\sim\lambda^3$ [7], but the focal geometries of conventional optical elements are not compatible with atomic localization $\simeq 100$ nm near microscopic photonic structures [2,3]. Moreover, spatially inhomogeneous energy shifts $U(\mathbf{r})$ on a subwavelength scale generally depend on the atomic internal state, limiting long-lived trap and coherence times due to single-photon scattering events with energy much larger than the recoil energy, and to spatially dependent frequency shifts for the components of atomic superpositions [8–10]. Nevertheless, important advances have been made by loading ultracold atoms into hollow-core optical fibers [11–15] and by trapping atoms in the evanescent fields of nanoscale waveguides [16–24].

Following the landmark realization of a nanofiber trap [21–23], in this Letter we report the implementation of a state-insensitive, compensated nanofiber trap for atomic cesium (Cs), as illustrated in Fig. 1 [10]. For our trap, differential scalar shifts δU_{scalar} between ground and excited states are eliminated by using "magic" wavelengths for both red- and blue-detuned trapping fields [25]. Inhomogeneous Zeeman broadening due to vector light shifts δU_{vector} is suppressed by way of pairs of counterpropagating red- and

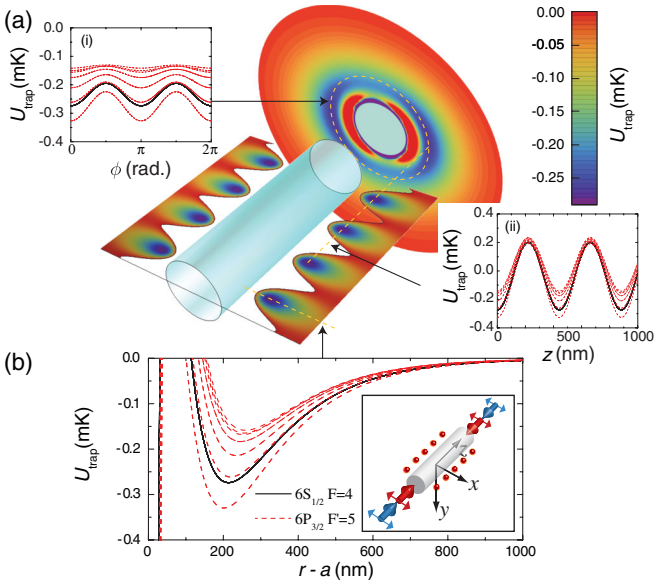

FIG. 1 (color). Adiabatic trapping potential U_{trap} for a state-insensitive, compensated nanofiber trap for the $6S_{1/2}$, $F = 4$ states in atomic Cs outside of a cylindrical waveguide of radius $a = 215$ nm [10]. U_{trap} values for the substates of the ground level $F = 4$ of $6S_{1/2}$ (excited level $F' = 5$ of $6P_{3/2}$) are shown as black (red-dashed) curves. Due to the complex polarizations of the trapping fields, the energy levels are not the eigenstates of the angular momentum operators, but rather superposition states of the Zeeman sublevels (see the Supplemental Material [26]). (a)(i) azimuthal $U_{\text{trap}}(\phi)$, (ii) axial $U_{\text{trap}}(z)$; and (b) radial $U_{\text{trap}}(r - a)$ trapping potentials. Input polarizations for the trapping beams are denoted by the red and blue arrows in the inset in (b).

blue-detuned fields. Here, the scalar and vector shifts refer to the respective spherical tensor components of the light-shift Hamiltonian parametrized by the dynamic polarizability tensor $\alpha(\omega)$ as discussed in the Supplemental Material [26].

The compensation of scalar and vector shifts results in a measured transition linewidth $\Gamma/2\pi = 5.7 \pm 0.1$ MHz for Cs atoms trapped 215 nm from the surface of an SiO_2 fiber of diameter 430 nm, which should be compared to the free-space linewidth $\Gamma_0/2\pi = 5.2$ MHz for the $6S_{1/2}$, $F = 4 \rightarrow 6P_{3/2}$, $F' = 5$ Cs transition. Probe light transmitted through the 1D array of trapped atoms exhibits an optical depth $d_N = 66 \pm 17$. From the measurements of optical depth and number N of atoms, we infer a single-atom attenuation $d_1 = d_N/N \simeq 0.08$. The bandwidth Γ_R for reflection from the 1D array is observed to broaden with increasing N, in direct proportion to the entropy for the multiplicity of trapping sites.

Our trapping scheme is based upon the analyses in Refs. [16–19] and the demonstrations in Refs. [21–23]. A dielectric fiber in vacuum with radius a smaller than a wavelength supports the "hybrid" fundamental mode HE_{11}, which carries significant energy in its evanescent field [27]. For linear input polarization at angle ϕ_0, an appropriate combination of attractive and repulsive HE_{11} fields creates a dipole-force trap external to the fiber's surface with trap minima at $\phi - \phi_0 = 0, \pi$.

Following these principles, we have designed a "magic compensation" scheme that traps both ground and excited states and greatly reduces the inhomogeneous broadening for atomic sublevels [10]. By contrast, uncompensated schemes do not provide a stable trapping potential for excited states and suffer large dephasing between ground states over a single vibrational period [21–23].

As shown in Fig. 1, our trap consists of a pair of counterpropagating x-polarized red-detuned beams at the magic wavelength [25] $\lambda_{\mathrm{red}} = 937$ nm to form an attractive 1D optical lattice. A second pair of beams at the magic wavelength $\lambda_{\mathrm{blue}} = 686$ nm with detuning δ_{blue} provides a repulsive contribution to U_{trap}, thereby protecting the trapped atoms from the short-ranged attractive surface interaction. To avoid a standing wave incommensurate with that at 937 nm, the blue-detuned beams have a relative detuning $\delta_{fb} = 382$ GHz and effectively yield linearly polarized light at all positions, where vector light shifts are suppressed by $\delta_{fb}/\delta_{\mathrm{blue}} \simeq 4 \times 10^{-3}$ [10]. The resulting potential U_{trap} allows for state-insensitive, 3D confinement of Cs atoms along a SiO_2 nanofiber for the $6S_{1/2}$ ground and $6P_{3/2}$ excited states.

We calculate the adiabatic potential U_{trap} in Fig. 1 from the full light-shift Hamiltonian (i.e., scalar, vector, and tensor shifts), together with the surface potential for Casimir-Polder interactions with the dielectric [10]. The red-detuned beams each have a power of 0.4 mW, while the blue-detuned beams each have a power of 5 mW. The trap depth at the minimum is $U_{\mathrm{trap}} = -0.27$ mK, located about

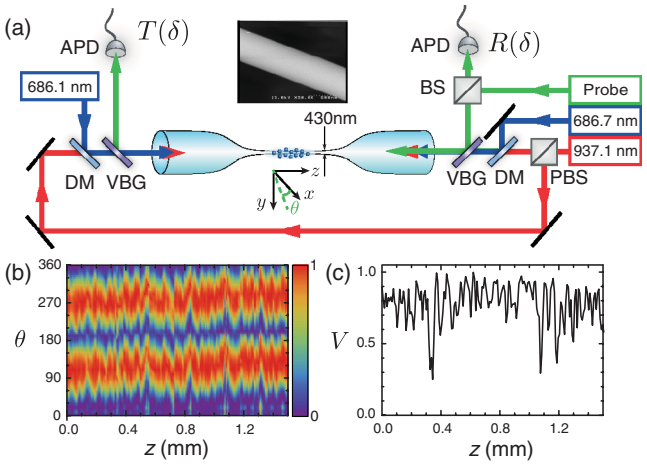

FIG. 2 (color). (a) Schematic of the setup for a state-insensitive, compensated nanofiber trap. VBG: volume Bragg grating. DM: dichroic mirror. PBS: polarizing beam splitter. APD: avalanche photodetector. The inset shows a SEM image of the nanofiber for atom trapping. (b) Angular distribution of the Rayleigh scattering intensity from the nanofiber as a function of the angle θ of the polarization for the incident probe field and of distance z along the fiber axis [36] (see Supplemental Material [26]). (c) Spatially resolved visibility V as a function of axial position z.

215 nm from the fiber surface, with trap frequencies $\{\nu_\rho, \nu_z, \nu_\phi\}/2\pi = \{199, 273, 35\}$ kHz.

An overview of our experiment is given in Fig. 2. A cloud of cold cesium atoms (diameter $\sim$1 mm) spatially overlaps the nanofiber. Cold atoms are loaded into U_{trap} during an optical molasses phase ($\sim$ 10 ms) and are then optically pumped to $6S_{1/2}$, $F = 4$ for 0.5 ms. The red- and blue-detuned trapping fields are constantly "on" throughout the laser cooling and loading processes with parameters comparable to those in Fig. 1.

For the transmission and reflection measurements, the trapped atoms are interrogated by a probe pulse (1 ms) with frequency ω_P, optical power $P_{\mathrm{probe}} \simeq 0.1$ pW, and detuning $\delta = \omega_P - \omega_A$ relative to the $F = 4 \leftrightarrow F' = 5$ transition frequency ω_A. The probe pulse is combined with the forward propagating trapping fields by a pair of volume Bragg gratings (VBGs) at the fiber input. The strong trapping beams are then filtered by a pair of VBGs at the fiber output, with the transmitted probe pulse monitored by a single-photon avalanche photodiode. The polarization of the probe laser is aligned along the trapping beams in order to maximize the overlap with the trapped atoms. We then shelve the atoms to $F = 3$ with a depumping pulse, and probe the fiber transmission with a reference pulse to determine the input power of the probe pulse.

As described in the Supplemental Material [26], the polarizations of the trapping and probe beams are aligned by observations of Rayleigh scattering [21]. From a simple model of the results in Figs. 2(b) and 2(c), we infer a transverse polarization vector $\vec{E}_{\mathrm{in}}(z = 0) = (E_x, iE_y)$ with

$\beta = \arctan(E_y/E_x) \simeq 12 \pm 3°$ for the probe beam. The principal axes of the polarization ellipse rotate in an approximately linear fashion along z in the trapping region by an angle $\phi(z) \simeq \phi_0 + [d\phi(z)/dz]\delta z$, where $\phi_0 \simeq 16°$ and $d\phi(z)/dz \simeq 12°/$ mm. These results are incorporated into our analysis of the measured transmission and reflection spectra of the trapped atoms (see Supplemental Material [26]).

The lifetime for atoms in our nanofiber trap is determined from the decay of the resonant optical depth $d_N \simeq N\sigma_0/A_{\text{eff}}$ as a function of storage time τ. Here, N is the number of trapped atoms, $\sigma_0 = \lambda^2/(2\pi)$ is the resonant absorption cross section, and $A_{\text{eff}} = P_{\text{probe}}/I_{\text{probe}}(\vec{r}_{\text{min}})$ is the effective optical mode area of the probe's evanescent wave. We observe that d_N decays exponentially with a time constant $\tau_0 = 12 \pm 1$ ms. With pulsed polarization-gradient cooling, the lifetime is extended to $\tau_{\text{PG}} = 140 \pm 11$ ms. We are currently characterizing the intensity and polarization noise spectra of the trapping fields to reduce parametric heating [28] with the goal of extending the trap lifetime towards the limit $\tau_r \sim 30$ s set by recoil heating.

Figure 3(a) displays the transmission spectra $T^{(N)}(\delta)$ for the 1D atomic array. The linewidth $\Gamma/2\pi = 5.8 \pm 0.5$ MHz is determined from a model (solid black line) incorporating fiber birefringence and linear atomic susceptibility (see Supplemental Material [26]) in the low density regime ($\tau = 299$ ms). The fitted line profile (solid red line) yields a maximum resonant optical depth $d_N = 66 \pm 17$ at $\tau = 1$ ms (see Supplemental Material [26]). Significantly, our magic, compensated scheme has no discernible shift of the transition frequency $\Delta_A/2\pi \simeq 0 \pm 0.5$ MHz relative to the free-space line center. The measured linewidths from four data sets average to $\Gamma/2\pi \simeq 5.7 \pm 0.1$ MHz, as compared to the free-space radiative linewidth $\Gamma_0/2\pi = 5.2$ MHz for the $6S_{1/2} \leftrightarrow 6P_{3/2}$ transition. By contrast, for a noncompensated scheme without magic wavelengths for Cs [21], the transition frequency is shifted by $\Delta_A/2\pi \simeq 13$ MHz and the linewidth is broadened to $\Gamma/2\pi \simeq 20$ MHz.

The broadening of the absorption linewidth above Γ_0 is predicted for our nanofiber trap because of the enhanced atomic decay into the forward and backward modes of the nanofiber at rate Γ_{1D} [29]. We estimate that an atom at the minimum of U_{trap} decays into the fiber at the rate $\Gamma_{1D}^{(1D)}/2\pi \simeq 0.32$ MHz, leading to a predicted linewidth $\Gamma_{\text{tot}}/2\pi \simeq 5.3$ MHz. Additional broadening arises from the tensor shifts of the excited $6P_{3/2}$, $F' = 5$ manifold ($\simeq 0.7$ MHz) and Casimir-Polder shifts ($\simeq 0.1$ MHz), as well as from technical noise of the probe laser ($\simeq 0.3$ MHz). While each of these contributions is being investigated in more detail, the spectra in Fig. 3 provide strong support for the effectiveness of our state-insensitive, compensated trapping scheme [10].

To determine the number of trapped atoms, we carry out a saturation measurement at a storage time $\tau = 1$ ms with $\delta = 0$ MHz. As shown in Fig. 3(b), we measure the power P_{abs} absorbed by the trapped atomic ensemble in the limit

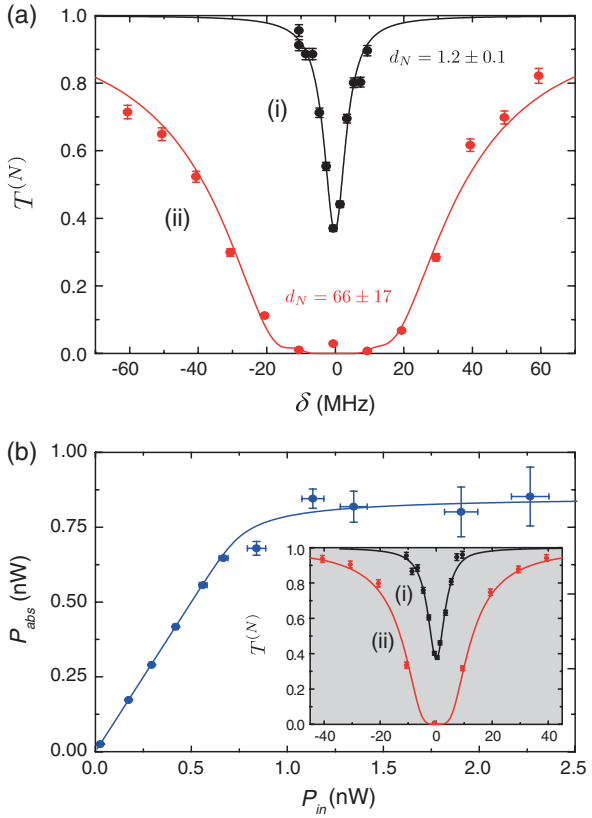

FIG. 3 (color). (a) Probe transmission spectra $T^{(N)}(\delta)$ for N trapped atoms as a function of detuning δ from the $6S_{1/2}$, $F = 4 \rightarrow 6P_{3/2}$, $F' = 5$ transition in Cs for x-polarized input. From fits to $T^{(N)}(\delta)$ (full curves), we obtain the optical depths d_N at $\delta = 0$ and linewidths Γ from a model that incorporates the polarization measurements in Figs. 2(b) and 2(c). $T^{(N)}(\delta)$ (i) at $\tau = 299$ ms with $d_N = 1.2 \pm 0.1$ and $\Gamma/2\pi = 5.8 \pm 0.5$ MHz and (ii) at $\tau = 1$ ms with $d_N = 66 \pm 17$. (b) Measurement of the power P_{abs} absorbed by the trapped atoms as a function of input power P_{in}, together with the associated optical depth $d_N = 18 \pm 2$ from curve (ii) (red line) of the inset, allows an inference of $N = 224 \pm 10$ [21]. The linewidth $\Gamma/2\pi = 5.5 \pm 0.4$ MHz and $d_N = 1.1 \pm 0.1$ are determined from curve (i) (black line) of the inset.

of high saturation $s = P/P_{\text{sat}} \gg 1$ [21]. As described in the Supplemental Material [26], the fitted curve (blue solid line) yields a number of trapped atoms $N = 224 \pm 10$. Together with the optical depth $d_N = 18$, we find an optical depth per atom $d_1 = (7.8 \pm 1.3) \times 10^{-2}$ for Fig. 3(b) [30]. A similar measurement in the Supplemental Material [26] with $d_N = 43 \pm 10$ and $N = 564 \pm 92$ yields $d_1 = (7.7 \pm 2.2) \times 10^{-2}$. These measurements of d_1 and Γ_{tot} were separated by four months and yield consistent results for the nanofiber trap. We thereby estimate $\Gamma_{1D}/2\pi \simeq 0.2$ MHz [31], similar to $\Gamma_{1D}^{(\text{th})}$.

The reflection from the 1D atomic array results from backscattering of the electromagnetic field within the 1D system [31]. The randomness in the distribution of N atoms among n_{site} trapping sites can greatly affect the reflection spectrum $R_N(\delta)$. For each random arrangement Λ of atomic occupations

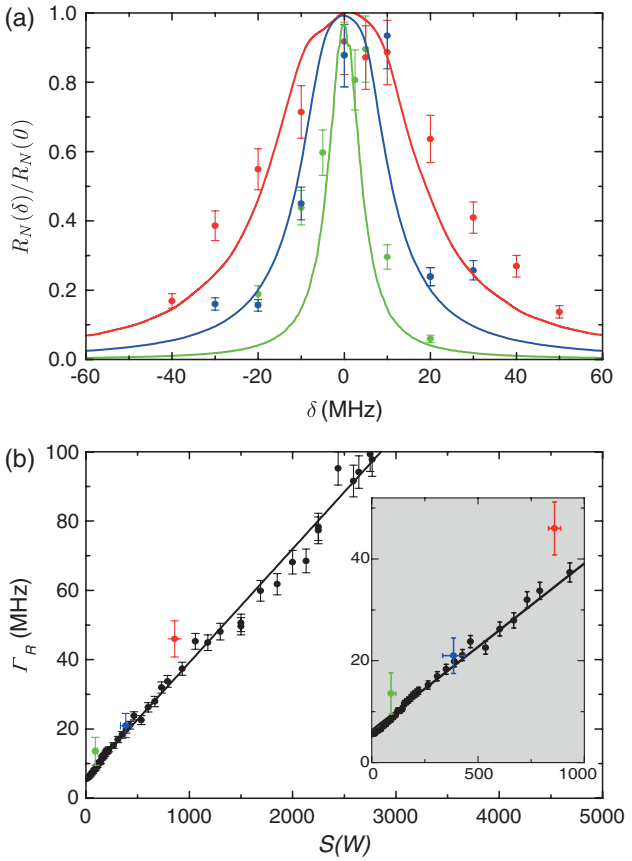

FIG. 4 (color). (a) Normalized reflection spectra $R_N(\delta)/R_N(0)$ from the 1D atomic array with $N = 14 \pm 2$ atoms (green points), $N = 79 \pm 13$ atoms (blue points), and $N = 224 \pm 10$ atoms (red points) randomly distributed across $n_{\text{site}} \simeq 4000$ sites. The solid lines are the spectra obtained from Monte Carlo simulations for $N \ll n_{\text{site}}$. (b) Simulated linewidth Γ_R of the reflection spectrum as a function of entropy $\mathcal{S}$. The error bars for the red, blue, and green data points include both statistical and systematic uncertainties. The black points are the results of a simulation with error bars representing numerical uncertainties. The solid line is a linear fit to the simulation points.

along the nanofiber (e.g., $\Lambda = \{1, 0, 0, \ldots, 1, 1, 0\}$), there is a unique narrow reflection spectrum whose resonance frequency δ_Λ is shifted from $\delta = 0$. δ_Λ depends sensitively on the configuration Λ due to the intricate interplay between coherent interference and dispersive phase shifts during the multipath walk of the probe field along the 1D atom array with noninteger $k_{\text{lattice}}/k_{\text{probe}}$, where k_{lattice} (k_{probe}) is the propagation constant for the lattice (probe) field. An ensemble average over Λ thus leads to a reflection spectrum $R_N(\delta)$ that is significantly broadened relative to the transmission spectra in Fig. 3.

In Fig. 4(a), we observe $R_N(\delta)$ from the 1D atomic array, where the measured Lorentzian linewidth Γ_R is significantly broadened from Γ_0 for large N (with $N \ll n_{\text{site}}$). The solid curves are for $R_N(\delta)$ from Monte Carlo simulations for the atomic distribution based on the transfer matrix formalism [32]. In order to quantify the microscopic state of disorder for the system, we define an entropy $\mathcal{S}$ for the 1D atomic array by $\mathcal{S} = \ln W$, where $W = \frac{n_{\text{site}}!}{N!(n_{\text{site}}-N)!}$ is the multiplicity for the atomic distribution in the 1D lattice. In Fig. 4(b), we find that the measured reflection linewidth Γ_R (colored points) as well as the linewidth Γ_R^{th} (black points) from the numerical simulation are proportional to the entropy $\mathcal{S}$ of the site-population statistics. These results demonstrate the strong modification of $R_N(\delta)$ due to randomness in the atomic distribution.

In conclusion, we have trapped atoms along a nanofiber by using a state-insensitive, compensated optical trap [10] to achieve an optical depth $d_N \simeq 66$. Compared to previous work with hollow-core fibers and nanofibers, the atoms are trapped with small perturbations to dipole-allowed transitions. Our scheme is thus well-suited to various applications, including the creation of 1D atomic mirrors for cavity QED, and investigations of single-photon nonlinearities and quantum many-body physics in 1D spin chains [31], as well as precision measurements of Casimir-Polder forces near a dielectric waveguide [33].

Currently, the maximum filling factor for sites over the 1 mm loading region is $\sim$19%, which can be improved with adiabatic loading and elimination of collisional blockade [34]. The vibrational ground state for axial motion in U_{trap} can be reached by introducing Raman sidebands on the 937 nm trapping fields [35]. The strong axial confinement in our trap implies the presence of a large anharmonicity in the vibrational ladder, which could provide a tool for experiments with single phonons. Furthermore, the design principles of our magic, compensated trap can be extended from simple "nanowires" to complex photonic crystal structures [3].

We gratefully acknowledge the contributions of D. Chang, I. Cirac, A. Gorshkov, L. Jiang, J. A. Muniz Silva, and E. Polzik. Funding at Caltech is provided by the IQIM, an NSF Physics Frontier Center with support of the Gordon and Betty Moore Foundation, by the AFOSR QuMPASS MURI, by the DoD NSSEFF program, and by NSF Grant No. PHY0652914. A. G. is supported by the Nakajima Foundation. The research of K. S. C. at KIST is supported by the KIST Institutional Programs (No. 2E22732 and No. 2Z03610). A. Goban, K. S. Choi, and D. J. Alton contributed equally to this work.

*Present address: Department of Physics, ETH Zürich, CH-8093 Zürich, Switzerland.
†Present address: Department of Physics and Astronomy, Northwestern University, Evanston, IL 60208, USA.

[1] H. J. Kimble, Nature (London) **453**, 1023 (2008).
[2] For a review, see K. J. Vahala, Nature (London) **424**, 839 (2003).
[3] M. Eichenfield, J. Chan, R. M. Camacho, K. J. Vahala, and O. Painter, Nature (London) **462**, 78 (2009).

[4] Y. B. Ovchinnikov, S. V. Shulga, and V. I. Balykin, J. Phys. B **24**, 3173 (1991).
[5] D. W. Vernooy and H. J. Kimble, Phys. Rev. A **55**, 1239 (1997).
[6] J. Burke, S.-T. Chu, G. W. Bryant, C. J. Williams, and P. S. Julienne, Phys. Rev. A **65**, 043411 (2002).
[7] N. Schlosser, G. Reymond, I. Protsenko, and P. Grangier, Nature (London) **411**, 1024 (2001).
[8] I. H. Deutsch and P. S. Jessen, Phys. Rev. A **57**, 1972 (1998).
[9] K. L. Corwin, S. J. M. Kuppens, D. Cho, and C. E. Wieman, Phys. Rev. Lett. **83**, 1311 (1999).
[10] C. Lacrôute, K. S. Choi, A. Goban, D. J. Alton, D. Ding, N. P. Stern, and H. J. Kimble, New J. Phys. **14**, 023056 (2012).
[11] M. J. Renn, D. Montgomery, O. Vdovin, D. Z. Anderson, C. E. Wieman, and E. A. Cornell , Phys. Rev. Lett. **75**, 3253 (1995).
[12] H. Ito, T. Nakata, K. Sakaki, M. Ohtsu, K. I. Lee, and W. Jhe, Phys. Rev. Lett. **76**, 4500 (1996).
[13] C. A. Christensen, S. Will, M. Saba, G.-B. Jo, Y.-I. Shin, W. Ketterle, and D. Pritchard, Phys. Rev. A **78**, 033429 (2008).
[14] P. Londero, V. Venkataraman, A. R. Bhagwat, A. D. Slepkov, and A. L. Gaeta , Phys. Rev. Lett. **103**, 043602 (2009).
[15] M. Bajcsy, S. Hofferberth, V. Balic, T. Peyronel, M. Hafezi, A. S. Zibrov, V. Vuletic, and M. D. Lukin, Phys. Rev. Lett. **102**, 203902 (2009).
[16] V. I. Balykin, K. Hakuta, F. Le Kien, J. Q. Liang, and M. Morinaga, Phys. Rev. A **70**, 011401 (2004).
[17] F. Le Kien, J. Q. Liang, K. Hakuta, and V. I. Balykin, Opt. Commun. **242**, 445 (2004).
[18] F. Le Kien, V. I. Balykin, and K. Hakuta, J. Phys. Soc. Jpn. **74**, 910 (2005).
[19] K. P. Nayak, P. N. Melentiev, M. Morinaga, F. Le Kien, V. I. Balykin, and K. Hakuta, Opt. Express **15**, 5431 (2007).
[20] G. Sague, E. Vetsch, W. Alt, D. Meschede, and A. Rauschenbeutel, Phys. Rev. Lett. **99**, 163602 (2007).
[21] E. Vetsch, D. Reitz, G. Sagué, R. Schmidt, S. T. Dawkins, and A. Rauschenbeutel, Phys. Rev. Lett. **104**, 203603 (2010).
[22] E. Vetsch, Ph.D. thesis, Johannes Gutenberg-Universität in Mainz, 2010.
[23] S. T. Dawkins, R. Mitsch, D. Reitz, E. Vetsch, and A. Rauschenbeutel, Phys. Rev. Lett. **107**, 243601 (2011).
[24] D. E. Chang, J. D. Thompson, H. Park, V. Vuletić, A. S. Zibrov, P. Zoller, and M. D. Lukin, Phys. Rev. Lett. **103**, 123004 (2009).
[25] J. Ye, H. J. Kimble, and H. Katori, Science **320**, 1734 (2008).
[26] See Supplemental Material at http://link.aps.org/supplemental/10.1103/PhysRevLett.109.033603 for a detailed discussion of nanofiber characterization, absorption analysis, and trap potential calculation.
[27] L. Tong, J. Lou, and E. Mazur, Opt. Express **12**, 1025 (2004).
[28] T. A. Savard, K. M. O'Hara, and J. E. Thomas, Phys. Rev. A **56**, R1095 (1997).
[29] F. Le Kien, S. Dutta Gupta, V. I. Balykin, and K. Hakuta, Phys. Rev. A **72**, 032509 (2005).
[30] Our measured optical depth per atom $d_1 \simeq 0.078$ is larger than $d_1 = 0.0065$ found in Ref. [21] due to our smaller nanofiber diameter, trap geometry, and reduced Γ_{tot}.
[31] D. E. Chang, L. Jiang, A. V. Gorshkov, and H. J. Kimble, New J. Phys. **14**, 063003 (2012).
[32] I. H. Deutsch, R. J. C. Spreeuw, S. L. Rolston, and W. D. Phillips, Phys. Rev. A **52**, 1394 (1995).
[33] J. M. Obrecht, R. J. Wild, M. Antezza, L. P. Pitaevskii, S. Stringari, and E. A. Cornell, Phys. Rev. Lett. **98**, 063201 (2007).
[34] T. Grünzweig, A. Hilliard, M. McGovern, and M. F. Andersen, Nature Phys. **6**, 951 (2010).
[35] A. D. Boozer, A. Boca, R. Miller, T. E. Northup, and H. J. Kimble, Phys. Rev. Lett. **97**, 083602 (2006).
[36] E. Vetsch, S. Dawkins, R. Mitsch, D. Reitz, P. Schneeweiss, and A. Rauschenbeutel, arXiv:1202.1494.